이학석사학위논문

High quality factor tuning-fork resonators with various resonance frequencies

높은 Q 인자와 다양한 공명진동수를 갖는 소리굽쇠 형태의 공명기에 대한 연구

2023년 2월

서울대학교 대학원
물리천문학부
오 찬 영

High quality factor tuning-fork resonators with various resonance frequencies

높은 Q 인자와 다양한 공명진동수를 갖는 소리굽쇠 형태의 공명기에 대한 연구

지도 교수 제 원 호

이 논문을 물리학 이학석사 학위논문으로 제출함

2023년 1월

서울대학교 대학원
물리천문학부
오찬영

오찬영의 이학석사 학위논문을 인준함

2023년 1월

위원장 _____ 이탁희 _____ (Seal)
부위원장 _____ 제원호 _____ (Seal)
위 원 _____ 김기훈 _____ (Seal)

Abstract

We demonstrate that the designed and fabricated tuning fork resonators have quality factors of about $10^3 \sim 10^4$ in the diverse frequency range from 50 Hz to 10 kHz in ambient condition. Metal and ceramic materials such as tantalum, steel, silicon nitride are used as resonator materials for high quality factors with minimal loss of mechanical energy. Resonators of various sizes with a tuning fork shape are realized by metal 3D printing method as well as metal machining process. We show that the increase in crystallinity of the 3D printed PLA tuning fork via annealing leads to an increase in quality factor, by which we confirm that the material to be used as a resonator should be with high crystallinity rather than an amorphous state. In addition, since the quality factor depends on the mass symmetry of both prongs for the case of a tuning fork type resonator, we improve the quality factor by matching the position and mass of the displacement-sensing accelerometer and the displacement-inducing actuator. The quality factor differences between predicted quality factor and measured one indicate that there are specific defects inside the material used as a resonator, which will be useful when the various-frequency tuning forks are employed as a highly sensitive force sensing resonator in the dynamic force microscopy

and spectroscopy.

Keywords: Tuning fork, Resonator, Quality factor, Resonance frequency

Student Number: 2020-23394

List of Figures

List of Tables

Table of Contents

Chapter 1

Introduction

In many fields of physics and engineering, physical and mechanical resonators are used for various purposes [1-5]. In particular, in the field of scanning probe microscopy (SPM), the role of the resonator used as a probe is very important. For example, the probe is critical for the surface scanning image quality or to determine the measurable force sensitivity between the surface and the tip in the dynamic atomic force microscopy (AFM) [6,7]. In the field of MEMS technology, micro/nano resonators have been widely studied because they have small size, a superior noise performance, and high mass sensing sensitivity compared to other types of resonators. In a resonator, there are two important parameters that can represent resonator, quality factor (Q factor) and resonance frequency. There are many reasons why quality factor and resonance frequency are important in the resonator. The quality factor and resonance frequency determine the response time(τ), $Q = \pi\tau f_0$, of the damped harmonic oscillator, thus determining the surface imaging speed in AFM. So, there are studies that actively control the q factor to optimize the imaging speed

[8,9]. Also, a resonator can be used as a force sensor to measure the interaction between the tip and the sample. The minimum force that the resonator can measure has a characteristic that depends on the Q factor, $F_{min} = \sqrt{\frac{2kk_BTB}{\pi f_0 Q}}$ where k is the spring constant of the cantilever, k_B is the Boltzmann constant, and B is the bandwidth [10]. That is, the higher the Q factor, the higher the force sensitivity appears. For example, in various studies, a quartz tuning fork (QTF) has been widely used as one of the resonators [11,12], with a high resonance frequency (32,768Hz) and a high Q factor (10^3~10^4) in air [13]. Meanwhile, the resonance frequency of the resonator is very important in fields such as rheology because the shear thinning or shear thickening phenomena in rheology and complex modulus G in viscoelastic materials rely on the frequency of stirring objects, at what resonance frequency the experiment is conducted is an important factor [14,15]. However, there are problems in that existing resonators are directly applied to fields such as rheology. First, the range of frequency in the existing rheology studies using rheometer and the resonance frequency of QTF or nano resonators are greatly different. The frequency region of the previous experiments using a rheometer is performed at several Hz to 10 kHz. However, in the QTF and micro/nano resonators, resonance frequencies usually have a high frequency range

from 20 kHz to several GHz. To apply research results and analysis using rheometer to AFM-based experiments, it is essential to develop a resonator having a low resonance frequency. Second, micro/nano resonators have a high surface to volume ratio, resulting in a significant decrease in Q factor in the room temperature and atmospheric pressure [16,17] . This means that it is necessary to develop a resonator having a high Q factor to measure the rheological properties of the sample at room temperature and pressure. Previously, Siria *et al* has conducted research on the nano rheology and nano tribology of water [18] and silicone oil [19] using accelerometer and centimetric aluminum tuning fork with more than thousands of Q factor, but they did not conduct a systematic study of the tuning fork type of resonator.

In this paper, the material and geometry are selected to have high Q ($10^3 \sim 10^4$) factors respectively in the fundamental resonance frequency in range of 50Hz to 10kHz. In particular, to have high Q factor, material groups (metal, ceramic) with low damping factor are used [20]. In this process, it is observed that the Q factor change significantly through mass balance using the mass and position of the accelerometer and piezo actuator. Furthermore, we compare experimental results with theoretical models as to which mechanism causes the loss of vibration energy

transferred to the tuning fork.

Chapter 2

Background Theory

2.1 Quality factor and Resonance frequency

A quality factor is defined as the ratio of energy stored to energy lost when a cycle of oscillation occurs. That is, the quality factor is a parameter that shows how much vibration energy is preserved without loss when an object oscillates. Basically, the quality factor is greatly influenced by the geometry of the vibrating resonator and external and internal factors. Resonance frequency is defined as the frequency at which an object oscillates at a relatively high amplitude. The resonance frequency can have various vibration modes depending on the geometry of the resonator, and is related to the density, Young's modulus, vibration mode and geometry of the material.

2.2 Analytical loss model for Quality factor

Basically, the resonator has several loss mechanisms. There are two main loss mechanisms, extrinsic loss and intrinsic loss. The extrinsic loss is the loss mechanism that strongly reflects the external factors such as air, absorbed material, and temperature. Many previous studies have already been conducted on the theoretical models of Q factor, and many comparisons with actual experimental data have been made. In this paper, we would like to explain some important theoretical models.

2.2.1 Air damping

When a resonator is oscillating in a fluid such as air, the resonator loses vibration energy by a viscous drag force of the fluid. Hosaka *et al* [21], derived the following equation by replacing cantilever beam with a set of continuous spheres with the same radius:

$$Q_{air} = \frac{\rho_b t W^2 \omega_n}{3\pi\eta W + \frac{3}{4}\pi W^2 \sqrt{2\rho_a \eta \omega_n}}, \quad (1)$$

where ρ_b is the density of the beam, ρ_a is the density of the air, η is the viscosity of the air, ω_n is the angular frequency of the nth flexural mode, and t is the thickness of the beam, and W is the width of the beam.

2.2.2 Thermoelastic damping

The thermoelastic damping (TED) is caused by a temperature gradient that appears in a oscillating beam resonator. The temperature gradient occurs between the compressed side and the stretched side around the neutral surface of the beam, resulting in loss in the form of irreversible heat flow. By Zener *et al*[23], this loss is expressed by the following equation:

$$Q_{TED} = \frac{\rho_b C}{E\alpha^2 T} \frac{1+(\omega\tau_z)^2}{\omega\tau_z}, \tag{2}$$

$$\text{with } \tau_z = \frac{\rho_b C T^2}{\pi^2 \kappa_{th}}, \tag{3}$$

where E is the Young's modulus of a material, α is the linear thermal expansion coefficient, T is the temperature, C is the specific heat capacity, κ_{th} is the thermal conductivity and τ_z is the relaxation time for thermoelastic damping.

2.2.3 Clamping loss

Generally, a resonator is used after being fixed using a fixture. Energy can be lost by the portion of the resonator held by this fixture, which is called clamping loss. Clamping loss occurs in a beam resonator with one or both ends fixed. The shear stress that occurs in the fixed end creates a

displacement, which causes elastic energy to pass from beam to support. The Q factor caused by the clamping loss mechanism is expressed in the following equation [22] :

$$Q_{clamp} = \kappa\left(\frac{L}{t}\right)^3, \tag{4}$$

where κ is the coefficient of the clamping loss depending on the properties of the material, and L is the length of the beam.

2.2.4 Phonon scattering loss

Crystalline solids with lattice structures have energy in the form of phonons inside the solid by thermal energy. When the crystalline beam vibrates, mechanical vibration locally perturbs the thermal phonons present in the thermal equilibrium state. Loss occurs in the process of returning to equilibrium:[24]

$$Q_{ph} = \frac{\rho_b v^2}{C_V t \gamma^2} \frac{1+(\omega\tau_{ph})^2}{\omega\tau_{ph}}, \tag{5}$$

$$\text{with } \tau_{ph} = \frac{3\kappa_{th}}{C_V v_n{}^2}, \tag{6}$$

where γ is Grüneisen's constant, v is the sound velocity, C_V is the heat

capacity per unit volume, and v_D is the Debye sound velocity.

2.2.5 Defect loss

Unlike the ideal perfect solid, all real solids have several kinds of defects inside [25]. The defect is divided into point defect (vacancies, interstitial atom) [26], line defect (dislocations) [27], surface defect (grain boundary) [28]. In a crystalline solid, Anelastic strain is produced by defects when a crystalline solid is deformed by external stress Loss caused by this anelastic strain can be formulated as follows, so-called 'Debye equation', through the standard linear solid model:

$$Q_{defect} = \frac{1+(\omega\tau_D)^2}{\Delta\omega\tau_D}, \quad (7)$$

where τ_D is the relaxation time for a defect, and Δ is the relaxation strength. Energy loss by defect is the main loss mechanism occurring in crystal structures such as metals and ceramics, and has been widely studied in various materials [24,29]. The loss of elastic energy occurs during the diffusion of defects (or defect pairs). In order for diffusion to occur, defects follow the following Arrhenius equation:

$$\tau_D = \tau_0 \exp\left(\frac{H}{k_B T}\right), \tag{8}$$

where H is activation enthalpy, and τ_0 is pre-exponential factor.

Chapter 3

Experimental procedure

In this paper, all resonators are shaped in the form of a tuning fork. We use polymer (poly lactic acid), metal (stainless steel 304, tool steel H13, tantalum), and ceramic (silicon nitride) as the resonator material.

3.1 Experimental setup

Figure 3.1 shows a schematic diagram of the experimental setup. When a voltage is applied to the piezo actuator with the function generator (Agilent technologies, 33120A), a mechanical displacement occurs in the piezo actuator. This causes the tuning fork to oscillate. the piezo actuator (PRYY 0398, PI) is attached to the other prong on the opposite side or the same side of prong to which the accelerometer (LIS302ALB, STMicroelectronics and ADXL 354, ANALOG DEVICES) is attached. The acceleration signal through the accelerometer is transmitted to the lock-in amplifier (EG&G Instruments, 7265 DSP Lock in amplifier), and the amplitude and phase of the signal are measured.

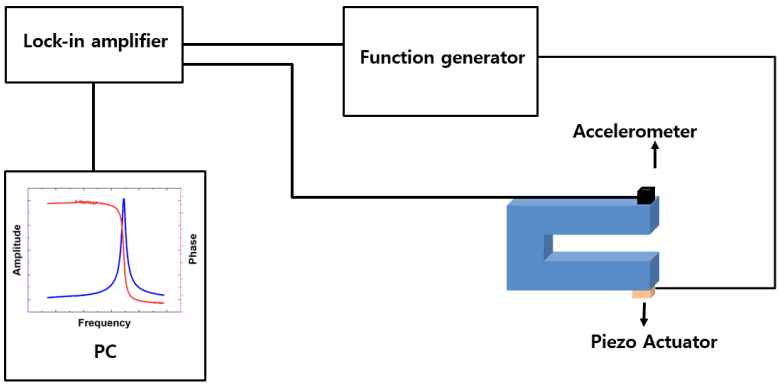

Figure 3.1: Schematic for experimental setup.

3.2 Fabricated tuning forks

3.2.1 3D printed polymer tuning forks

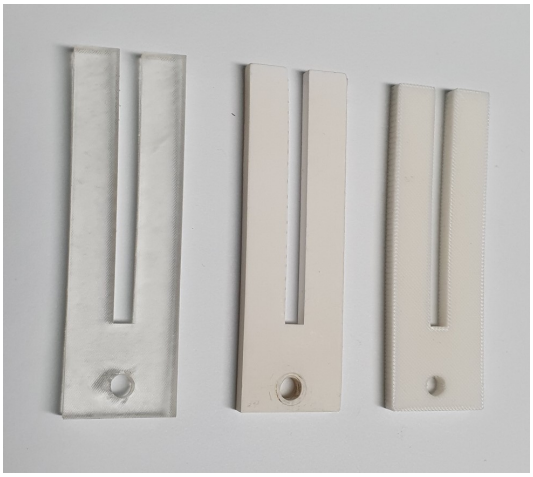

Figure 3.2: 3D printed polymer tuning forks. From left to right, UV clear resin, Rigid 10k, PLA tuning fork.

We manufacture tuning forks using poly lactic acid (PLA) through 3d printing in a fused deposition modeling (FDM) 3d printer (Style NEO-A22C, CUBICON) and using Rigid 10k, UV clear resin through 3d printing in a stereo lithography apparatus (SLA) 3d printer (Form 3, Formlabs). For PLA tuning forks, to check the change in the Q factor by increasing the crystallinity of the material through annealing, these seven tuning forks are subjected to annealing of 110 °C for 60 min. Then we turn off the furnace and waited for a day for the temperature inside the furnace to drop to room temperature. The polymer tuning forks (PLA, Rigid 10k, UV clear resin) are made of the same size: length = 75 mm, thickness = 12 mm, and width = 6 mm. Figure 3.2 shows 3d printed polymer tuning forks.

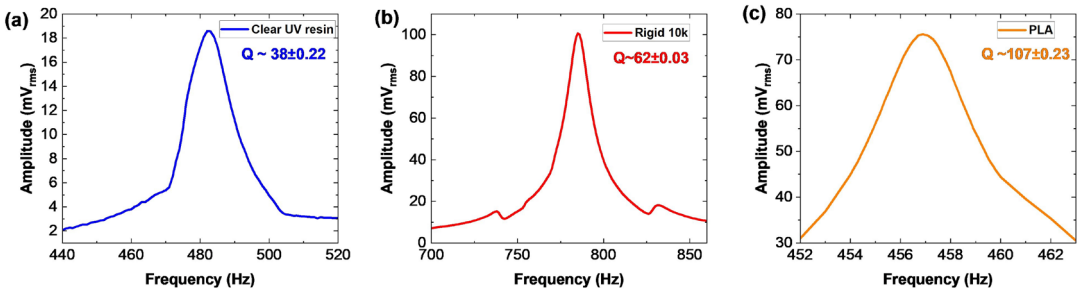

Figure 3.3: Resonance curves of 3d printed polymer tuning forks.

Figure 3.3 shows the Q factor of 3d printed polymer tuning forks. Each

Q factor is approximately 100 or less similar.

3.2.2 Metal and ceramic tuning forks

Metal and ceramic materials generally known to have low damping factors are selected as the resonator materials used. Our metal tuning forks are manufactured in two different methods, 3D printing and metal machining. 3d printing method is applied only for tool steel H13 because materials that can be manufactured with a 3d printer are mainly limited to steel. using a metal 3d printer (metal X, Markforged). Metal 3d printing is carried out in a chamber filled with inert gas to prevent metal oxidation. When metal powder is sprayed on the build platform in the form of a thin layer, a sample is produced through the process of melting and hardening by applying heat with a laser. The bare part printed from the 3d printer is immersed in a washing solution to remove binding materials. After that, it is sintered at 1030°C for 30 minutes. The printing sample is quenched in the air. Immediately after air cooling, printing samples are tempered at 600°C. Other material group (stainless steel 304, tantalum, silicon nitride, single crystal copper [100] and poly crystal copper) is manufactured using laser cutting and wire cutting by processing through metal

machining process after making a plate-shaped sample. Figure 3.4 and Figure 3.5 show tuning forks made of metal and ceramic.

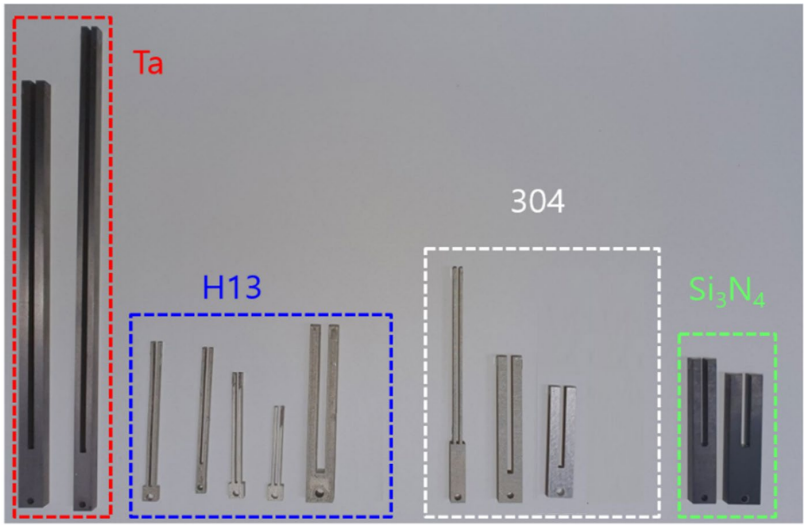

Figure 3.4: Tuning forks made using 3d printing and metal machining process. H13 is tool steel H13, 304 is stainless steel 304.

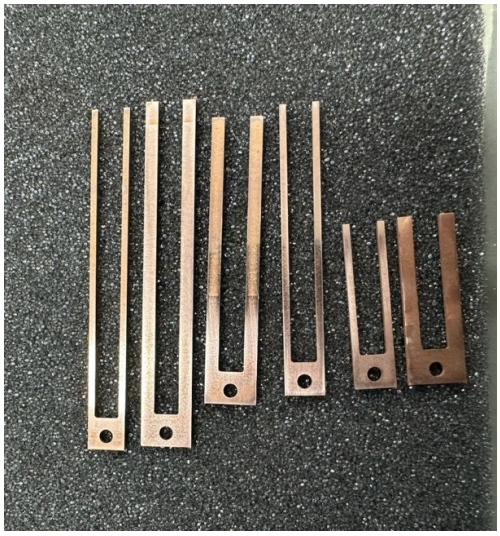

Figure 3.5: Tuning forks made using single crystal copper [100] (Crystal bank, Pusan university)

Chapter 4

Result and Discussion

4.1 Material selection and Resonance curve

In many studies, the results of research on cantilevers made of polycrystalline, single crystal diamonds and amorphous polymers show

the selection criteria for the types of solids used as resonators [3,4,30]. For example, it is known that polymer has a large damping factor compared to metal and ceramic [31]. Compared to materials with crystal structures, an amorphous structure of polymer generates more loss in the process of transferring elastic energy. In particular, the FDM-based 3d printing process affects the crystallinity of the printed sample. Differential scanning calorimetry (DSC) results show that annealing of 3d printed PLA samples increases the crystallinity of PLA compared to before, resulting in lower loss tangents [32].

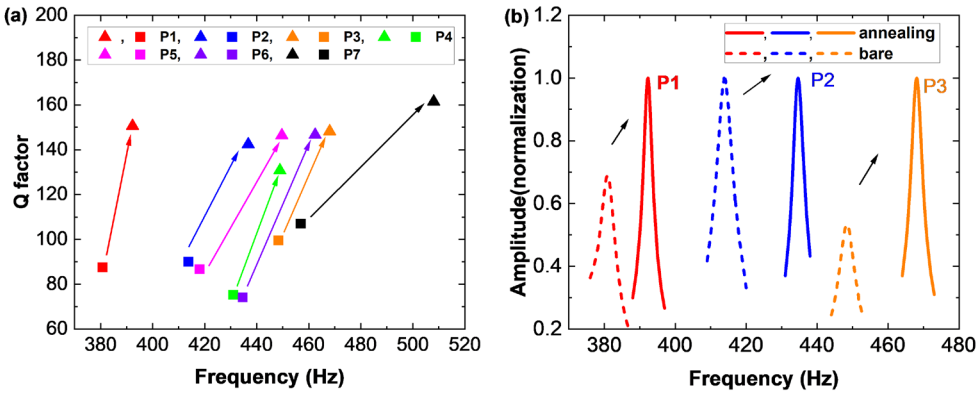

Figure 4.1: Resonance curves of PLA tuning forks. P1 to P7 are PLA tuning forks printed in the same size. (a) The Q factors is increased after annealing (triangle) compared to before annealing (square) (b) Resonance curves of tuning forks. Solid lines mean before annealing, and dashed lines mean after annealing. Normalization is calculated based on the curve for each after annealing.

Figure 4.1 shows the resonance curves and q factors of the PLA tuning forks before and after annealing. In the FDM 3d printing method, when PLA is ejected from a nozzle with a temperature of about 120 °C, the PLA cools rapidly at room temperature. In this process, PLA changes from semi-crystalline to amorphous, and annealing restores the crystallinity of PLA through recrystallization. This result shows that the increase in crystallinity through annealing in PLA tuning fork increases the Q factor.

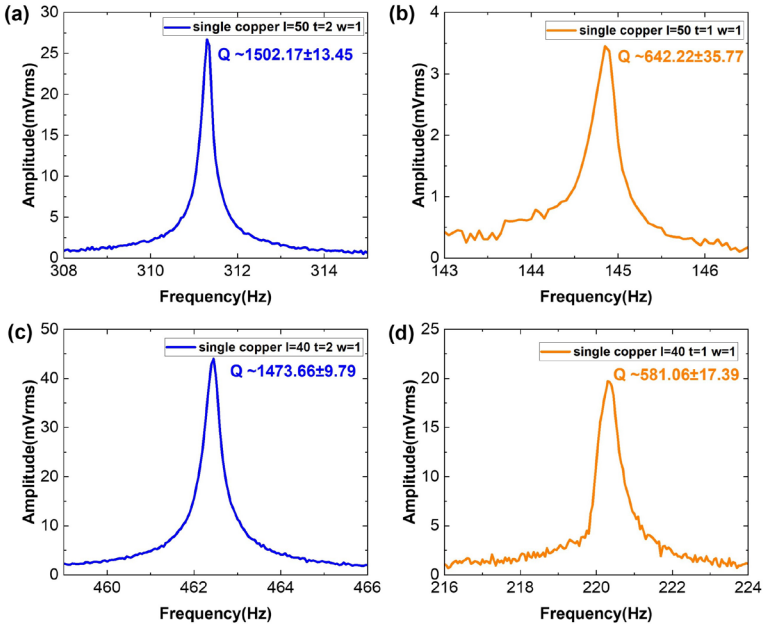

Figure 4.2: Resonance curves of single crystal copper. (a) length=50mm, thickness=2mm, width=1mm. (b) length=50mm, thickness=1mm, width=1mm. (c)

length=40mm, thickness=2mm, width=1mm. (d) length=50mm, thickness=1mm, width=1mm.

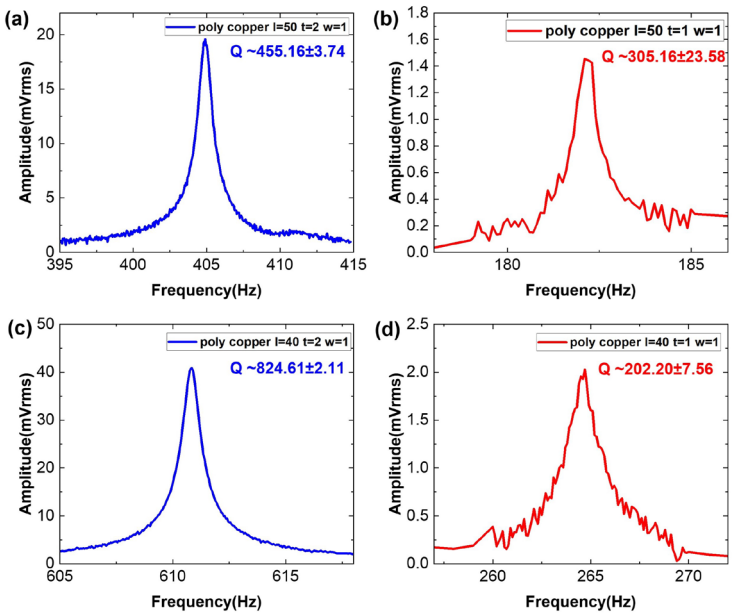

Figure 4.3: Resonance curves of oxgen free poly crystal copper. (a) length=50mm, thickness=2mm, width=1mm. (b) length=50mm, thickness=1mm, width=1mm. (c) length=40mm, thickness=2mm, width=1mm. (d) length=50mm, thickness=1mm, width=1mm.

In addition, we measure the Q factor of tuning forks made with the same design using single crystal copper and polycrystalline copper. Figure 4.2 and figure 4.3 show the difference between the resonance frequency and Q factor of the single crystal and polycrystalline copper tuning forks. A Q

factor is 2 to 3 times higher in single crystal copper tuning fork than in polycrystalline copper tuning fork. Through the above results, we conclude that using a material with higher crystallinity even if it is the same material is advantageous in obtaining a higher Q factor. So we manufacture resonators using crystalline materials and easily manufactured methods (3d printing method and metal machining process).

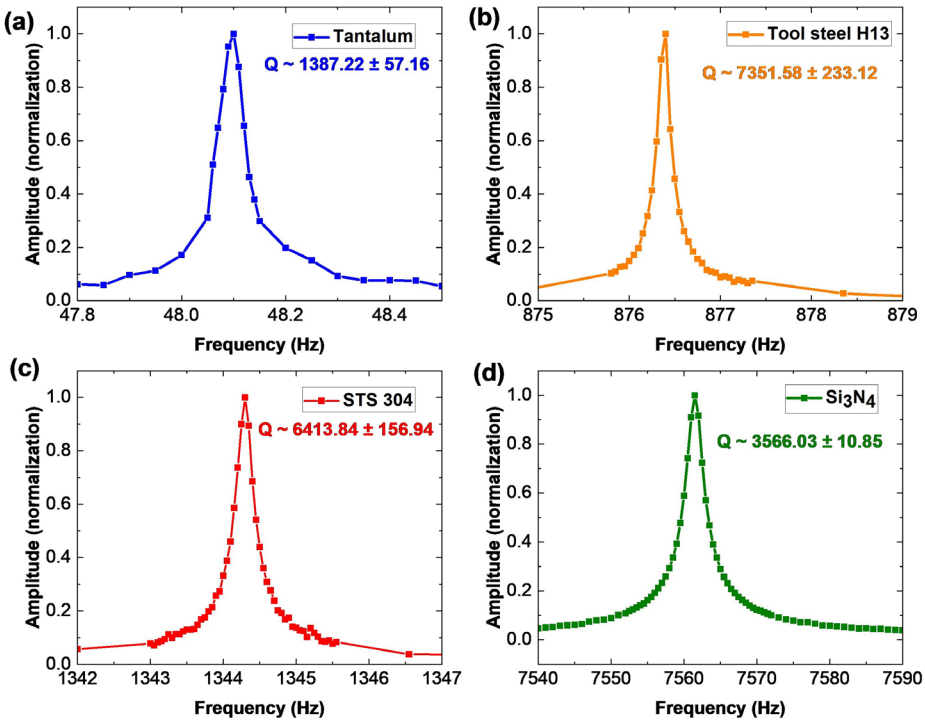

Figure 4.4: Resonance curves of 4 high Q factor tuning forks. (a) tantalum, (b) tool steel H13, (c) stainless steel 304, (d) silicon nitride.

Figure 4.4 shows the resonance curves for 4 tuning forks made with tantalum, tool steel H13, stainless steel 304 and silicon nitride. The Q factors and dimension for these tuning forks are shown in Table 1. Each resonance curve is normalized with respect to its maximum amplitude. The oscillation amplitude of tuning forks is hundreds of nanometers to a few micrometers. Tuning forks can also have amplitudes of tens of nanometers or several nanometers and oscillate at amplitudes below (~500pm) [19].

Also, even if the tuning fork has the same resonance frequency, tuning fork have various lengths and thicknesses by (9). We use Finite difference time domain (FDTD) simulation using COMSOL multiphysics to check how the Q factor changes even if it has a similar resonance frequency. Figure 4.5 shows the resonance curves and Q factor when the length and thickness are adjusted to have a similar resonance frequency (~880Hz) for the H13 tuning fork with l=50mm t=3mm w=6.5mm among the tuning forks we manufactured.

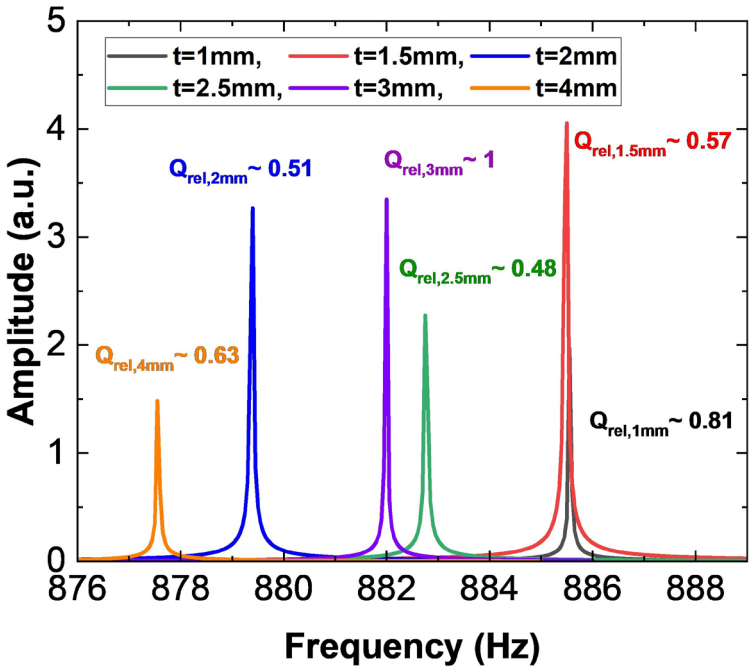

Figure 4.5: Resonance curves and Q factors of tuning forks having a thickness t=1mm, 1.5mm, 2mm, 2.5mm, 3mm, 4 mm and a corresponding length when the resonance frequency is about 880 Hz. $Q_{rel,t}=\frac{Q_t}{Q_{max}}$ where Q_t is the Q factor of the tuning fork with the thickness of t and Q_{max} is the Q factor when t = 3mm.

This result shows the difference in the Q factor for the thickness of the tuning fork. Experimentally, we also confirmed that there is a length to thickness ratio with a higher Q factor, even if it has a similar resonance frequency, as shown in Table 1. However, the calculated Q factor in COMSOL simulation is at least 4 times higher than the measured one

because only the geometrical factor and internal damping are considered in simulations.

4.2 Resonance frequency and Young's modulus

Table 1 shows the dimensions of the tuning fork and the type of materials used. The dimensions were determined using the following results by Euler-Bernoulli equation so that the fundamental mode could be obtained near a specific calculated fundamental mode resonance frequency [33]:

$$f_0 = \frac{t}{4\pi L^2}\sqrt{\frac{E}{0.2427\rho_0}}, \tag{9}$$

According to previous results, there is a result that resonance frequency is reduced when a tip is attached to the prong of QTF because the mass of prong increases [34,35]. In the case of mechanical resonators, the frequency of resonance decreases because the mass of prong increases by the accelerometer and piezo actuator. A slight correction is required to calculate the original resonance frequency of the tuning fork. When a small mass is attached on a prong of the tuning fork, the shift in its resonance frequency is given as follows:[35]

$$\Delta f_0 = \frac{-\Delta m}{2m} f_0, \quad (10)$$

where m is a prong mass, Δm is an added mass. In Figure 4.6 (a), The measured resonance frequency and corrected resonance frequency are shown. The accelerometers and actuators used weigh from 0.12 g to 0.4 g, respectively, almost the same as each other.

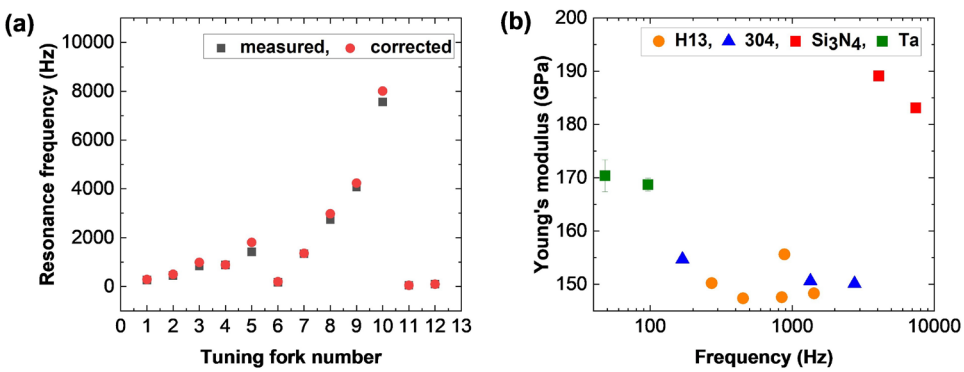

Figure 4.6: (a) Experimentally measured resonance frequency (black square) and corrected resonance frequency (red circle). In tuning fork number, 1~5 are tool steel H13, 6~8 are stainless steel 304, 9~10 are Si_3N_4, 11~12 are Ta. (b) Young's modulus of tuning forks calculated from resonance frequency.

We can calculate the Young's modulus of the tuning fork through corrected resonance frequency. Figure 4.6(b) shows the Young's modulus calculated by the measured resonance frequency. The Young's modulus of tantalum tuning fork was 170.37 ± 2.99 GPa and 168.73 ± 1.23 GPa,

respectively, matching the known Young's modulus values of 170 GPa~190 GPa, and the silicon nitride tuning fork was also measured within the range of 160 GPa~290 GPa, which is the modulus values of 189.13 ± 0.01 GPa and 183.13 ± 0.01 GPa, respectively. In the case of stainless steel 304 and tool steel H13, the estimated Young's modulus from the measured resonance frequency is 147 GPa to 155 GPa, which is lower than the previously well-known Young's modulus value of 190 GPa to 210 GPa. There are two possible reasons for this difference. First, both steels show lower density values (H13-7.38g/cm^3, STS 304-7.46g/cm^3) than known density values (H13-7.8g/cm^3, STS 304-8.00/cm^3). When the porosity occurs in a material, the density decreases and the modulus decreases at the same time [36]. This suggests that certain defects may exist inside the tuning fork production process. Second, in the process of measuring the resonance frequency, an accelerometer and an actuator must be attached, so damping by a sensor may occur. When damping occurs, the resonance frequency becomes lower, which indicates a result of a lower Young's modulus value according to (9)

TABLE Ⅰ. Q factors and resonance frequency of tuning forks measured at room temperature and atmospheric pressure.

Material	Length(mm)	Thickness(mm)	Width(mm)	Resonance frequency(Hz)	Q
H13	50	1	3	271.1	2343
H13	38	1	3	450.9	2571
H13	27	1	3	845.35	1575
H13	50	3	6.5	881.9	7364
H13	20	1	3	1422.9	2000
Ta	146	2	6	48.1	1387
Ta	126	3	6	96.55	2820
STS304	61	1	3	168.75	1436
STS304	40	3	6	1344	6689
STS304	27	3	4	2747.2	2212
Si_3N_4	30	3	6	4077	6142
Si_3N_4	25	4	6	7561.5	3566

4.3 Mass balance

A tuning fork ideally has a geometry in which two prongs have symmetry. If the tuning fork vibrates in-plane out of phase mode, the center of mass of the tuning fork does not move due to the symmetrical structure, and the energy lost to the support part does not exist. However, when the tip or sensor is attached to the prong, the symmetry of the tuning fork is broken and energy loss occurs, resulting in a decrease in the value of the Q factor. If the effective mass of the two prongs is equal to each other by additional mass, the Q factor is restored again, which is called the 'mass balance' [37]. In the case of the QTF, it is known that the symmetry of the tuning fork is broken by the tip attached to the prong, so that the resonance frequency is shifted and the quality factor is greatly reduced by damping [19]. We confirm similar results in our experiment. The Q factor reduction by the mass symmetry broken is examined by varying actuator positions. As shown in Figure 4.7(a), in the case of positions C and B, the geometric symmetry of the tuning fork is broken by the accelerometer and actuator. Position C has a lowest Q factor because the accelerometer and actuator are located on the same line, which means that the symmetry is more broken than position B. However, when an actuator with almost the same mass as an accelerometer is attached to

position A, the Q factor becomes much larger than other positions. In particular, it was confirmed that the difference between the Q factor was very large when the ratio of the mass of the prong and the mass of the sensor was small. In other words, when the size of the tuning fork is small or a low density material is used, mass balance is essential for a high Q factor.

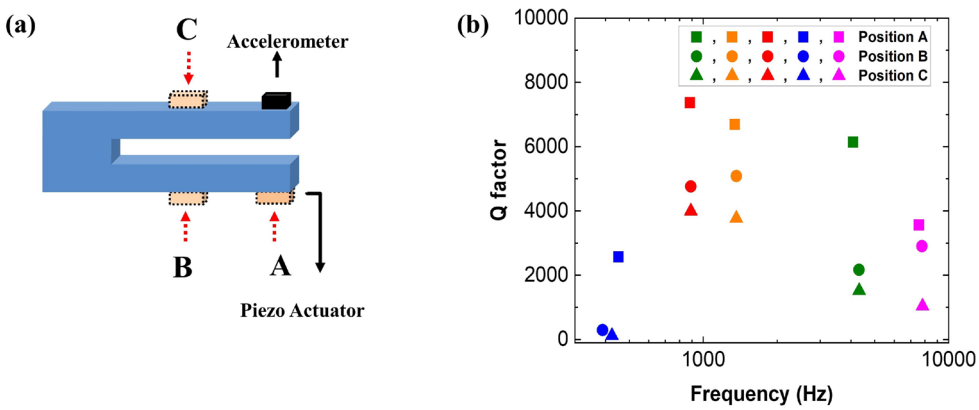

Figure 4.7: (a) Position of accelerometer and actuator in tuning fork. The mass of the accelerometer and piezo actuator is from 0.1g to 0.4g, which is the same for each experiment. LIS302ALB and PRYY 0398 are used for 0.1g mass balance, and ADXL 354 and cube pzt are used for 0.4g mass balance. The mass ratio of each prong and accelerometer is 19.5% (H13, 450.9Hz), 1.58% (H13, 881.9Hz), 2.39% (STS 304, 1344Hz), 7.95% (Si_3N_4, 7561.5Hz), 11% (Si_3N_4, 4077Hz). (b) The Q factors when the position of the actuator is placed at A (square), B (circle), C (triangle) while the position of the accelerometer is fixed.

4.4 Dissipation in metal and ceramic tuning fork

We have introduced several loss mechanisms in section Table 2 shows the physical properties of tuning fork materials used in our experiment. Figure 4.8 shows the difference between the calculated value (air loss, thermoelastic loss, phonon scattering loss) and the measured value. Even we conduct our experiment in air, there is a discrepancy between the theoretical loss model by air and the measured one. This can be interpreted as being hardly affected by air because the resonator has a low surface to volume ratio, unlike a micro/nano resonator. Second, thermoelastic and clamping loss mechanism theoretically shows a strong dependence, $Q_{TED} \propto \frac{t^3}{L^2}$, $Q_{clamp} \propto \left(\frac{L}{t}\right)^3$, on the length and thickness of the tuning fork, but the measured results do not follow the geometric dependence these models exhibit. Also, as all of the materials used, stainless steel, tantalum, and silicon carbide, are solid crystals, it can be expected that there will be loss mechanism by phonon when vibration occurs. However, this loss mechanism also shows a large discrepancy with the measured values. This means that air loss, thermoelastic loss, phonon scattering loss and clamping loss do not affect the elastic energy loss of the tuning fork. This is a very different result from the results of

previous experiments on QTF [38] or silicon cantilever [39], in which clamping loss or thermal loss were found to be the main cause of loss. Unlike quartz or silicon single crystal, the metal and ceramic materials used in the experiment have more fundamental loss mechanism.

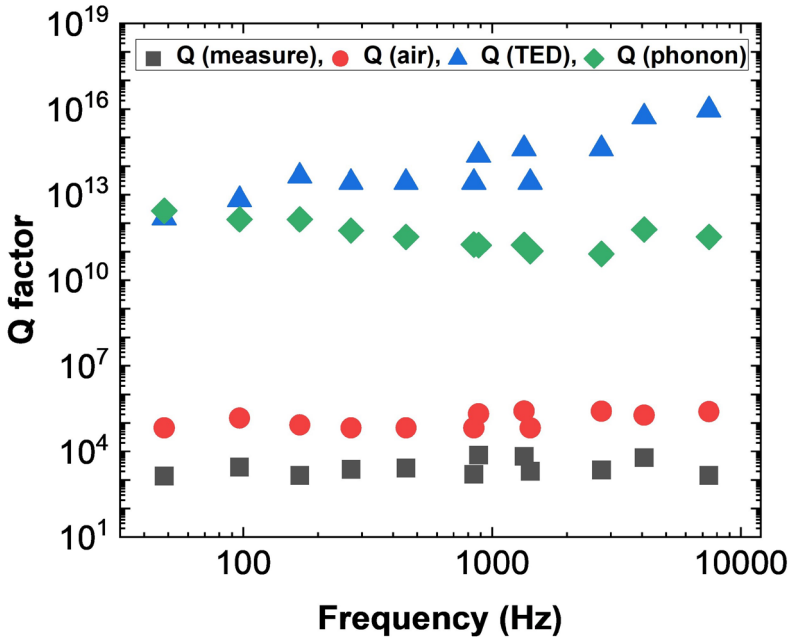

Figure 4.8: Theoretically calculated Q_{air} (red circle), Q_{phonon} (green diamond), Q_{TED} (blue triangle) and measured $Q_{measure}$ (black square). The experiment was conducted at normal pressure, at 22 C and at 40% RH

There can be many defects inside the crystal, and these defects can act as the main factor limiting the Q factor of the resonator, or the factor that

increases damping. There are various types of defects, such as interstitial atom, vacancy, and dislocation. Stainless steel 304 has a chemical composition of Cr (19%), Ni (9%), N (0.05%), C (0.04%), and a face-centered cubic (fcc) crystal structure. In this structure, interstitial solute atoms in fcc metals occupy octahedral interstitial sites. One possible loss mechanism in this structure is the Finkelshtein and Rosin relaxation (FR relaxation) process discovered by the Finkelshtein and Rosin [40]. Energy loss is caused by the reorientation of interstitial–substantial atom (IA–SA) pairs or interstitial–interstitial atom (IA–IA) pairs. On the other hand, tool steel H13 has a chemical composition of Cr (4.7%), Mo (1.3%), Si (0.8%), V (0.8%), C (0.3%), and a body-centered cubic (bcc) crystal structure. In bcc metals, defect loss occurs by a relaxation process called Snoek relaxation [41]. Particularly, there is a possibility that various types of defects may have occurred inside the material during the 3d printing method or metal machining process. We therefore infer that the internal defects are the main limiting factor for the Q factor of the tuning fork.

TABLE Ⅱ. Constant values of each substance used for each energy loss (Q_{air}, Q_{ph}, Q_{TED}, Q_{defect})

Parameter	Stainless steel 304	Tantalum	Silicon nitride	H13
$\rho_b(kg/m^3)$	7461	16680	3051	7381
$C(J/kg \cdot K)$	500	140	660	460
$\alpha(10^{-6}/K)$	17.2	6.4	3.21	12.6
E(GPa)	150	170	190	150
$\kappa_{th}(W/mK)$	16.2	57.5	20.5	26
$C_V(10^6 J/m^3K)$	3.73	2.32	2.01	3.39
v_D(m/s)	3575.18	2275.76	6245.03	3692.82
γ	2.0	1.75	0.39	2.0

Chapter 5

Conclusion

We measure Q factors for a tuning fork-type resonator with a resonance frequency in the range of 50Hz to 10kHz. The tuning forks are made of stainless steel 304, tool steel H13, tantalum, and silicon carbide using a 3d printer and metal machining process. Resonance frequencies and Q factors are measured by attaching an accelerometer and an actuator to the prong of the tuning fork. The Q factors of tuning forks are measured in the range of $10^3 \sim 10^4$ at room temperature and atmospheric pressure regardless of the resonance frequency. By making the weight and position of the sensors attached in the tuning fork form symmetrical, the mass balance effect of recovering the Q factor was observed. In addition, by comparing the theoretical calculated values and measured values of several loss mechanisms, we guess that the main loss mechanism that limits the Q factor in steel tuning fork is due to certain kinds of defects. The defect concentration inside the resonator used by the accelerometer Q measurement method could also be estimated, which showed values

similar to those previously known. We expect that this tuning fork type of resonator can be used in the field of rheology or tribology research in the AFM experiments.

Bibliography

[1] A. Hajjaj, N. Jaber, S. Ilyas, F. Alfosail, and M. I. Younis, International Journal of Non-Linear Mechanics **119**, 103328 (2020).

[2] J. Rieger, A. Isacsson, M. J. Seitner, J. P. Kotthaus, and E. M. Weig, Nature communications **5**, 1 (2014).

[3] P. Ovartchaiyapong, L. Pascal, B. Myers, P. Lauria, and A. Bleszynski Jayich, Applied Physics Letters **101**, 163505 (2012).

[4] V. P. Adiga, A. Sumant, S. Suresh, C. Gudeman, O. Auciello, J. Carlisle, and R. W. Carpick, Physical Review B **79**, 245403 (2009).

[5] D. Czaplewski, J. Sullivan, T. Friedmann, D. Carr, B. Keeler, and J. Wendt, Journal of Applied Physics **97**, 023517 (2005).

[6] S. Liu and Y. Wang, Scanning **32**, 61 (2010).

[7] F. J. Giessibl, Review of Scientific Instruments **90**, 011101 (2019).

[8] T. Sulchek, R. Hsieh, J. Adams, G. Yaralioglu, S. Minne, C. Quate, J. Cleveland, A. Atalar, and D. Adderton, Applied Physics Letters **76**, 1473 (2000).

[9] M. Lee, J. G. Hwang, J. Jahng, Q. Kim, H. Noh, S. An, and W. Jhe, Journal of Applied Physics **120**, 074503 (2016).

[10] T. Stowe, K. Yasumura, T. Kenny, D. Botkin, K. Wago, and D.

Rugar, Applied Physics Letters **71**, 288 (1997).

[11] M. Lee, J. Jahng, K. Kim, and W. Jhe, Applied physics letters **91**, 023117 (2007).

[12] M. Todorovic and S. Schultz, Journal of applied physics **83**, 6229 (1998).

[13] J.-M. Friedt and É. Carry, American Journal of Physics **75**, 415 (2007).

[14] S. Gürgen, M. C. Kuşhan, and W. Li, Progress in Polymer Science **75**, 48 (2017).

[15] M. Guvendiren, H. D. Lu, and J. A. Burdick, Soft matter **8**, 260 (2012).

[16] S. S. Verbridge, H. G. Craighead, and J. M. Parpia, Applied Physics Letters **92**, 013112 (2008).

[17] S. S. Verbridge, R. Ilic, H. G. Craighead, and J. M. Parpia, Applied Physics Letters **93**, 013101 (2008).

[18] L. Canale, J. Comtet, A. Niguès, C. Cohen, C. Clanet, A. Siria, and L. Bocquet, Physical Review X **9**, 041025 (2019).

[19] A. Lainé, L. Jubin, L. Canale, L. Bocquet, A. Siria, S. H. Donaldson, and A. Niguès, Nanotechnology **30**, 195502 (2019).

[20] D. Chung, Journal of materials science **36**, 5733 (2001).

[21] H. Hosaka, K. Itao, and S. Kuroda, Sensors and Actuators A: Physical **49**, 87 (1995).

[22] Z. Hao, A. Erbil, and F. Ayazi, Sensors and Actuators A: Physical **109**, 156 (2003).

[23] C. Zener, Physical review **53**, 90 (1938).

[24] V. B. Braginskiĭ, V. P. Mitrofanov, and V. I. Panov, *Systems with small dissipation* (University of Chicago Press, 1985).

[25] M. Blanter, I. Golovin, H. Neuhäuser, and H. Sinning, (Springer Berlin, 2007).

[26] H. Numakura, K. Kashiwazaki, H. Yokoyama, and M. Koiwa, Journal of alloys and compounds **310**, 344 (2000).

[27] I. Golovin and S. Golovin, Le Journal de Physique IV **6**, C8 (1996).

[28] G. Miles and G. Leak, Proceedings of the Physical Society (1958-1967) **78**, 1529 (1961).

[29] R. Schaller, G. Fantozzi, and G. Gremaud, in *Materials science forum* (trans tech Publications, 2001).

[30] N. von Windheim, D. W. Collinson, T. Lau, L. C. Brinson, and K. Gall, Rapid Prototyping Journal (2021).

[31] M. F. Ashby and D. CEBON, Le Journal de Physique IV **3**, C7 (1993).

[32] N. Chikkanna, S. Krishnapillai, and V. Ramachandran, The International Journal of Advanced Manufacturing Technology **119**, 1179 (2022).

[33] A. N. Cleland, *Foundations of nanomechanics: from solid-state theory to device applications* (Springer Science & Business Media, 2013).

[34] D. Hussain, J. Song, H. Zhang, X. Meng, W. Yongbing, and H. Xie, IEEE Sensors Journal **17**, 2797 (2017).

[35] J. Zhang and S. O'shea, Sensors and Actuators B: Chemical **94**, 65 (2003).

[36] B. D. Flinn, R. K. Bordia, A. Zimmermann, and J. Rödel, Journal of the European Ceramic Society **20**, 2561 (2000).

[37] B. P. Ng, Y. Zhang, S. W. Kok, and Y. C. Soh, Ultramicroscopy **109**, 291 (2009).

[38] P. Patimisco, A. Sampaolo, V. Mackowiak, H. Rossmadl, A. Cable, F. K. Tittel, and V. Spagnolo, IEEE transactions on ultrasonics, ferroelectrics, and frequency control **65**, 1951 (2018).

[39] S. Schmid, K. Jensen, K. Nielsen, and A. Boisen, Physical Review B **84**, 165307 (2011).

[40] K. Rosin and B. Finkelshtein, Doklady Akademii Nauk SSSR **91**, 4 (1953).

[41] J. Snoek, Physica **8**, 711 (1941).

국문 초록

공명기는 자연과학과 공학의 다양한 분야에서 여러 목적으로 사용되어왔다. 특히 원자력 힘 현미경과 같은 주사 탐침 현미경 분야에서 공명기는 샘플의 표면을 측정하거나 샘플과 팁 사이의 힘을 측정하는데 있어서 매우 중요한 역할을 한다. 공명기를 힘을 측정하는 힘 센서로 사용하는 경우에 미세한 힘을 측정하기 위해서 높은 Q 인자를 갖는 것은 매우 중요하다. 특히 유변학과 같은 분야에서 물질의 점성, 탄성, 전단 박화 등은 측정하는 진동수의 영향을 크게 받는다. 하지만 기존에 존재하던 수정진동자나 나노/마이크로 공명기의 경우에는 그 크기로 인해 수십 kHz이상의 매우 높은 고유 주파수를 가지거나 상온 상압의 환경에서 Q 인자가 매우 감소하는 특징을 보였다. 우리는 이 문제를 해결하고자 본 연구에서 금속과 세라믹 물질을 사용하여 상온 상압에서 1000~10000 사이의 Q 인자를 가지면서 50Hz~10kHz 범위의 고유주파수를 갖는 소리굽쇠 형태의 공명기를 개발했다. 공명기를 제작하기 위해서 3d 프린팅 방법과 판금가공방식을 사용했으며, 측정은 가속도 측정 센서와 압전변환기를 사용한 역학적 측정 방식을 사용했다. 또한 열처리 이전과 열처리 이후의 PLA 튜닝포크Q 인자 결과와 단결정, 다결정 튜닝포크의 Q 인자 결과를 통해 물질의 결정성이 Q 인자에 큰 영향을 미침을 확인하였다. 본 연구를 통해, 우리는 공명기 제작 방식과 제작 물질에 대한 기준을 제시할 수 있었고,

또한 개발된 공명기들은 동적 힘 현미경 분야에서 높은 민감도와 다양한 공진주파수를 갖는 공명기로 유용하게 사용될 것으로 기대된다.

주요어: 튜닝포크, 공진기, 공명 진동수, Q 인자

학번: 2020-23394